# Low-Energy Backgrounds in Solid-State Phonon and Charge Detectors

Daniel Baxter,[1,2] Rouven Essig,[3] Yonit Hochberg,[4,5] Margarita Kaznacheeva,[6] Belina von Krosigk,[7,8] Florian Reindl,[9,10] Roger K. Romani,[11] and Felix Wagner[12,13]

[1]Quantum Division, Fermi National Accelerator Laboratory, Batavia, Illinois, USA; email: dbaxter9@fnal.gov

[2]Department of Physics and Astronomy, Northwestern University, Evanston, Illinois, USA

[3]C.N. Yang Institute for Theoretical Physics, Stony Brook University, Stony Brook, New York, USA; email: rouven.essig@stonybrook.edu

[4]Racah Institute of Physics, Hebrew University of Jerusalem, Jerusalem, Israel; email: yonit.hochberg@mail.huji.ac.il

[5]Laboratory for Elementary Particle Physics, Cornell University, Ithaca, New York, USA

[6]Department of Physics, TUM School of Natural Sciences, Technical University of Munich, Garching, Germany; email: margarita.kaznacheeva@tum.de

[7]Kirchhoff Institute for Physics, Heidelberg University, Heidelberg, Germany; email: bkrosigk@kip.uni-heidelberg.de

[8]Institute for Astroparticle Physics, Karlsruhe Institute of Technology (KIT), Karlsruhe, Germany

[9]Institute of High Energy Physics (HEPHY), Austrian Academy of Sciences, Vienna, Austria

[10]Atominstitut (ATI), TU Wien, Vienna, Austria; email: florian.reindl@tuwien.ac.at

[11]Department of Physics, University of California, Berkeley, California, USA; email: rkromani@berkeley.edu

[12]Department of Physics, ETH Zurich, Zurich, Switzerland; email: felix.wagner@phys.ethz.ch

[13]ETH Zurich-PSI Quantum Computing Hub, Paul Scherrer Institute, Villigen, Switzerland

## Keywords

## Abstract

Solid-state phonon and charge detectors probe the scattering of weakly interacting particles, such as dark matter and neutrinos, through their low recoil thresholds. Recent advancements have pushed sensitivity to eV-scale energy depositions, uncovering previously unseen low-energy excess backgrounds. While some arise from known processes such as thermal radiation, luminescence, and stress, others remain unexplained. This review examines these backgrounds, their possible origins, and parallels to low-energy effects in solids, an understanding of which is essential for interpreting particle interactions at and below the eV scale.

## Contents

## 1. INTRODUCTION

The rapid advancement of low-threshold detectors over the last decade has unlocked energy ranges that were previously inaccessible, revealing new backgrounds that previously were not well-understood. The way that these effects manifest in different detectors varies, but in general, all detectors with thresholds that are sufficiently low to be sensitive to energies below ∼100 eV measure a steeply rising event rate with decreasing energy that we refer to here as a low-energy excess (LEE) (1). While there are commonalities in the various LEEs measured by different experiments using similar detector technologies, a common origin to explain all LEE rates—for example, a dark matter (DM) signal—is inconsistent with the data. Furthermore, the origins of the LEEs in phonon-sensitive detectors and charge-sensitive detectors are distinct. The modeling and mitigation of these LEEs are crucial for the continued advancement of rare event detection at the eV scale, in particular for the direct detection of sub-GeV DM and for the precision measurement of coherent elastic neutrino–nucleus scattering (CEvNS).

An LEE has been observed in various solid-state DM and CEνNS detectors for at least a decade, but often at detector thresholds where systematic modeling was poor and background simulations had not yet been validated. The first unambiguous observations of an LEE came from the EDELWEISS (2) and CRESST (3) Collaborations in 2019. In a 6-day surface run with a 33.4-g Ge bolometer, the EDELWEISS Collaboration observed an LEE above a flat radiogenic background rate of $\sim 10^3$ dru ($\equiv$ counts per kilogram per day per keV) down to a 60-eV threshold (2). Shortly after, the CRESST-III experiment, operated deep underground at the Laboratori Nazionali del Gran Sasso (LNGS), released its first low-threshold run from a 23.6-g $CaWO_4$ crystal operated for more than a year (3.64-kg-day total exposure after cuts) (3); in these low-background data, the CRESST-II investigators observed a significant LEE below 200 eV, down to a 30-eV analysis threshold. Notably, both of these cryogenic detectors measure the total energy deposited in the crystal by observing the total phonon energy following an event.

In light of these convincing LEE observations, prior results sensitive to sub-keV energy depositions were revisited, and what previously had been widely considered to be systematic effects near threshold were newly viewed as suspect. This included earlier results from a CRESST-style prototype detector for CEνNS detection, NUCLEUS (4, 5), which in 2017 marked the first measurement of a cryogenic LEE in the literature. The reinterpretation also included charge-sensitive detectors where single-electron rates had long exceeded theoretically predicted levels, including SuperCDMS-HVeV (6) and SENSEI at MINOS (7); follow-up measurements from DAMIC at SNOLAB (8) and EDELWEISS HV (9) displayed similar behavior. Around this time, attempts to find a unifying explanation for these LEEs (10) were unsuccessful (11, 12) but yielded some interesting ideas on testing the nature of the LEEs (13, 14). With a single common explanation ruled out, the DM and CEνNS fields embarked on a multiyear campaign to share data and expertise to categorize and eliminate LEE backgrounds—an effort encapsulated by the EXCESS Workshop Series (1). While outside the scope of this review, gaseous and liquid detectors have long suffered from LEE backgrounds in charge-sensitive (15–18) and heat (19) channels. There is a near-total overlap of the statistical handling of such backgrounds and a similar narrative of long-lived metastable states releasing energy over time.

In this review, we summarize the status of the various solid-state LEEs, including what is known about their behavior in different types of detectors, what remains to be understood, and ongoing efforts toward modeling and mitigation. Without a comprehensive understanding, the various sources of LEEs will severely hinder the low-threshold DM and CEνNS detection programs over the next decade. Beyond these two applications, there is increasing evidence that LEEs may present a challenge for solid-state quantum computing technologies, which are intrinsically sensitive to any type of environmental interaction.

## 2. LOW-THRESHOLD DETECTION

The search for light (sub-GeV mass) DM particles and the study of CEνNS kinematically require detectors that are capable of precisely measuring eV-scale energy transfers to their bulk material. DM and neutrinos can transfer energy to the target nuclei or the target electrons and (depending on the material) produce electrons, scintillation photons, and phonons (20–27). In this review, we focus on low-threshold experiments that use solid-state monocrystalline targets with either phonons or charge as their primary signal channel. Some phonon-based experiments combine their primary channel with a secondary channel (phonon plus charge/scintillation) as a means of particle discrimination between electron and nuclear recoils and/or for surface-event rejection. For an overview on particle discrimination and surface-event rejection, we refer the reader to References 28–30. **Figure 1** illustrates the working principle of the relevant detectors.
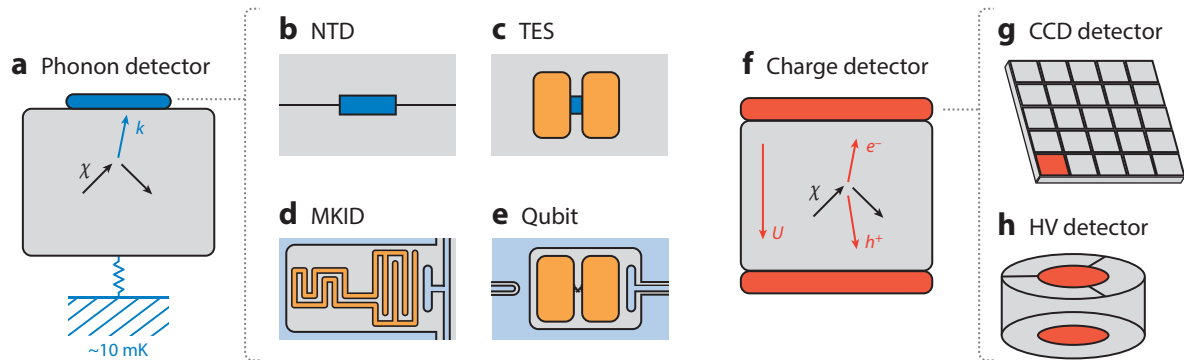
**Figure 1**

Relevant detectors. (*a–e*) Phonon-based detectors, including (*b*) NTDs, (*c*) TESs, (*d*) MKIDs, and (*e*) qubits, wherein interactions create phonons, which are registered by a phonon sensor (*blue*). (*f–h*) Charge-collecting detectors, including (*g*) CCD detectors and (*h*) HV detectors, wherein particle interactions in the crystal bulk (*gray*) will generate *e–h* pairs that are drifted by an electric field toward electrodes at the top or bottom (*red*). Abbreviations: CCD, charge-coupled device; HV, high-voltage; MKID, microwave kinetic inductance detector; NTD, neutron transmutation doped; TES, transition edge sensor.

## 2.1. Measuring Phonons

Energy depositions of sufficient magnitude in a cryogenic crystal absorber create a population of nonthermal phonons. These decay instantaneously (∼ns) to acoustic phonons of the Debye frequency ($\hbar\omega \sim 80$ meV in Si) and lower, which propagate ballistically through the crystal. Within microseconds they decay to thermal energies, leading to a temperature increase of the crystal. The crystal then cools back to its equilibrium temperature through a thermal link with a heat bath (31). Sensing this phonon population is fundamentally limited by the energy of thermal phonons (thermal noise). Many characteristics of detectors that crucially influence their sensitivity are strongly temperature dependent—for instance, heat capacities and thermal couplings ($\propto T^3$ for insulators and $\propto T$ for metals) and the superconducting state and its equilibrium quasiparticle (QP) population. Phonon sensors are therefore typically operated at temperatures of approximately 10 mK in dilution refrigerators. Typical heat capacities of the system are on the order of a few picojoules per millikelvin, and thermal couplings are on the order of several hundred picowatts per millikelvin, leading to pulse lengths of milliseconds to hundreds of milliseconds. The initially deposited energy can originate from the recoil of a massive particle or radiation interactions in the crystal, sensor, or their interface, but also from stress or vibrations. Sensing this energy can follow two strategies depicted in **Figure 1*a***: either collecting the prompt athermal phonon population or measuring the temperature increase. We discuss several sensor types below.

A neutron transmutation doped (NTD) sensor (**Figure 1*b***) is a semiconductor thermistor, often using Ge, which is strongly coupled to the absorber crystal, sensing the thermal phonon population. Its sensitivity and timing resolution depend strongly on the heat capacity and thermal coupling of the absorber crystal. Typical energy thresholds of such sensors are well above 1 keV with timing resolutions on the order of 100 ms to seconds (30). Transition edge sensors (TESs) are superconducting films operated in transition to their normal conducting state (**Figure 1*c***). The strong temperature dependence of the electrical resistance in this state enables sensitivity to microkelvin-scale temperature fluctuations. Additional fully superconducting phonon collectors can amplify the signal: The athermal phonon population generates Bogoliubov QPs in the collector that are successively trapped in the TES, improving the phonon collection efficiency without adding to the heat capacity or thermal coupling. Optimized sensors can reach energy thresholds

on the eV scale and submillisecond timing resolutions (32, 33). The combination of tungsten TES (W-TES) and aluminum fins used in such detectors is known as a quasiparticle-trap-assisted electrothermal-feedback TES (QET) (34).

The creation of QPs in superconductors can be leveraged as a fully athermal readout scheme. This principle is used in microwave kinetic inductance detectors (MKIDs), superconducting resonators with frequencies in the gigahertz regime (**Figure 1d**). The presence of QPs shifts the resonator frequency, resulting in a measurable signal. MKIDs have achieved energy thresholds <100 eV and timing resolutions of approximately 100 μs (35, 36). Alternatively, a superconducting quantum interference device (SQUID) capacitor circuit can be operated as a qubit (**Figure 1e**), keeping a coherent quantum state for $\gtrsim$100 μs that is read out and manipulated through microwave pulses. The coherence and transition energies of such qubits are sensitive to single QPs tunneling through the Josephson junctions, a mechanism that has been studied extensively in the quantum computing literature (37–39). Prototypes using such qubits as sensitive particle detectors have been studied, and some optimized designs have been proposed (40–42).

While the calibration of low-threshold phonon detectors is challenging, multiple methods have been employed. Calibrations using electronic energy deposition [∼6-keV $\gamma$-rays from $^{55}$Fe (e.g., 43, 44); ∼eV optical photon sources (e.g., 32, 45)], nuclear events (46, 47), and drifted charges within the detector (48) have all been used to calibrate low-threshold phonon detectors with broadly self-consistent results. Significantly above the trigger threshold and below the saturation point of a given detector, this calibration essentially serves to measure the linear scale factor (in some contexts, the phonon collection efficiency) between a given energy deposited in the detector's phonon system and the size of the observed signal. Broadly, the response of these low-threshold phonon detectors seems to be well-understood.

## 2.2. Measuring Charges

Traditional charge-sensitive solid-state DM detectors are made from either Si or Ge. When energy is deposited in the semiconductor crystal, it can excite electrons from the valence band to the conduction band, creating electron–hole (e–h) pairs. The energy required to create one e–h pair in a semiconductor is typically larger than the bandgap because some energy will be lost to phonons. The average energy required to create an e–h pair at room temperature is ∼3.6 eV for Si and ∼2.9 eV for Ge. Using an applied electric field, e–h pairs in the bulk are drifted to the edges of the detector, where they are measured (**Figure 1f**). The charge collection efficiency and number of measured charge carriers are influenced by factors such as impurities, defects, and drift field strength. If the electric field is weak or the time for the carriers to travel across the crystal is long, an electron from the conduction band can recombine with a hole in the valence band, resulting in the loss of both charge carriers and reducing the detectable signal. The ionization yield is higher for electron recoils compared to nuclear recoils. We therefore discuss the energy measured by a charge detector in units of electron-equivalent energy (eV$_{ee}$), as the recoil energy valid for an electron interaction, to distinguish from phonon detectors that measure the total energy deposited independently of the type of interaction.

A charge-coupled device (CCD) consists of many coupled capacitors, which effectively divide up the detector into pixels (**Figure 1g**). Any e–h pairs produced in the bulk are drifted toward a buried channel, an extremum of the potential close to the detector surface. This channel can be p-type, in which case it stores holes, or n-type, in which case it stores electrons. Gates on either the front or back side of the device move the charges in each capacitor to its neighbor through synchronized clocked voltages until they reach the serial register, a row of pixels across which the charges can be transferred to the readout amplifier. In a conventional CCD, the total charge in each pixel is measured once before it is discarded. Electronic noise from the CCD output

amplifier adds both high- and low-frequency readout noise. High-frequency readout noise can be reduced by correlated double sampling (49), but low-frequency noise remains and results in a measurement uncertainty for each pixel charge of ∼2–3 $e$–$h$ rms per pixel. In a skipper CCD, the readout amplifier is modified by coupling a floating-gate output stage to a small-capacitance sense node. In this way, multiple nondestructive measurements of the same pixel charge can be performed, also reducing the low-frequency noise and allowing a measurement of pixel charge to a precision of ≪1 $e$–$h$ rms per pixel.

In the case of cryogenic charge-sensitive devices as depicted in **Figure 1*b***, two scenarios should be distinguished. In the first, the applied bias voltage is on the order of a few volts, resulting in an electric field strength of ≲1 V cm$^{-1}$. Electrodes on the crystal surfaces, instrumented with high-impedance charge amplifiers (see **Figure 1*b***), measure the image charge collected, providing a direct measure of the deposited energy used to produce $e$–$h$ pairs. Alternatively, larger voltages on the order of 100 V can be applied, resulting in electric field strengths of >100 V cm$^{-1}$; such devices are commonly referred to as high-voltage (HV) detectors. The purpose of the high voltage is to amplify the charge signal in the form of secondary phonons, exploiting the Neganov–Trofimov–Luke (NTL) effect (50, 51). As $e$–$h$ pairs drift across the crystal, they quickly reach terminal velocity, long before reaching a surface. Due to significant charge–phonon interactions, the excess work done on the carriers is transferred to the crystal lattice in the form of NTL phonons. Consequently, the total phonon energy (measured using sensors described in Section 2.1) scales directly with the bias voltage and provides a strongly amplified phonon signal that dwarfs the original charge signal. With bias voltages ∼100 V, the total NTL phonon energy per initial $e$–$h$ pair is ∼100 eV, allowing for resolutions ≪1 $e$–$h$ and functionally enabling quantized $e$–$h$ pair readout.

## 3. SUMMARY OF OBSERVED LOW-ENERGY EVENTS

LEE backgrounds have been observed in multiple low-threshold experiments. These experiments are optimized to sense charge or phonon signals, and some experiments are sensitive to both. Below, we discuss the LEEs observed in phonon detectors in Section 3.1 and those in charge detectors in Section 3.2.

### 3.1. Low-Energy Events in Phonon Detectors

Phonon LEE backgrounds have been measured in different sensor types, with various materials, and at setups with strongly varying background levels. These measurements exhibit several properties that are commonly observed in various experiments (as summarized in **Table 1**):

**Table 1    Common properties of LEE backgrounds observed in various experiments**

| Experiment | 1. Rise | 2. Decay | 3. Ionization | 4. Coincidence | 5. Absorber |
|---|---|---|---|---|---|
| CRESST-III (43, 63) | Yes | Yes | NA | No | Yes |
| NUCLEUS (5, 64) | Yes | Yes | NA | NA | Yes |
| TESSERACT (45, 53) | Yes | Yes | NA | No | Yes |
| SuperCDMS-CPD (33, 65) | Yes | Yes | NA | NA | NA |
| EDELWEISS (9, 66, 67) | Yes | Yes | No | NA | Yes |
| RICOCHET (68) | Yes | NA | No | NA | NA |
| BULLKID (35) | No | NA | NA | NA | NA |
| Mannila et al. (69) | Yes | Yes | NA | NA | NA |

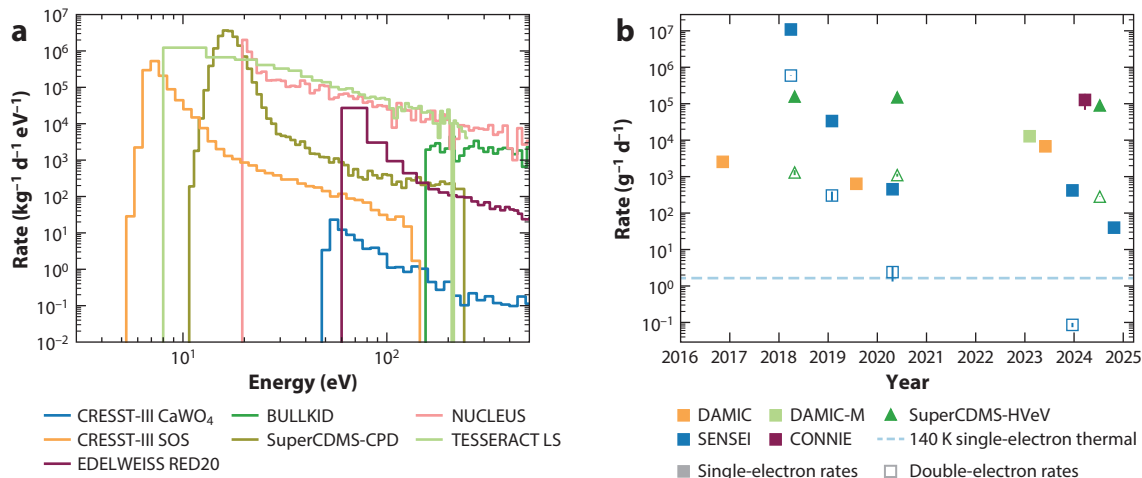Abbreviations: LEE, low-energy excess; NA, not applicable.

**Figure 2**

Low-energy excess rates. (*a*) Spectra observed by various phonon-based cryogenic experiments: CRESST-III [CaWO$_4$ (43) and SOS (32); W-TES, LNGS], EDELWEISS RED20 (Ge, NTD, surface) (2), BULLKID (Si, MKID, surface) (52), SuperCDMS-CPD (Si, W-TES, surface) (33), NUCLEUS (Al$_2$O$_3$, W-TES, surface) (4), and TESSERACT LS configuration (Si, W-TES, surface) (53). (*b*) Single-electron rates (*solid shapes*) and double-electron rates (*open shapes*) in Si for each experiment with sensitivity to individual electron–hole production; data from the DAMIC (8, 54, 55), SENSEI (7, 56–59), DAMIC-M (60), CONNIE (61), and SuperCDMS-HVeV (6, 48, 62) experiments are organized by the date of first arXiv posting. Squares indicate CCD experiments at ∼140 K, triangles indicate cryogenic experiments at <1 K, and the dashed line indicates the upper limit of the dark rate from bulk thermal single-electron excitations for a CCD operated at 140 K according to Equation 1. Abbreviations: CCD, charge-coupled device; LNGS, Laboratori Nazionali del Gran Sasso; LS, low stress; MKID, microwave kinetic inductance detector; NTD, neutron transmutation doped; SOS, Si on Sapphire; W-TES, tungsten transition edge sensor.

1. The excess background rate rises steeply toward lower energies, typically observable below ∼100–200 eV. In most datasets, the rise of the background does not follow a single exponential or power-law model but requires combinations thereof.

2. The excess background rate monotonically decays with time after the cooldown of the setup, and subsequent warm-up cycles partially or completely reset the rate.

3. Detectors sensitive to both phonons and charges observe excess background events only in the form of phonons. The background sources thus appear to couple exclusively to the phonon system with no simultaneous ionization.

4. Detectors placed in a joint housing (i.e., without light-tight shielding against each other) do not observe the excess background events in coincidence.

5. Detectors that can discriminate between absorber and sensor events observe a significant share of the background excess events depositing energy in the phonon system of the absorber. Some events have been observed to deposit energy directly in the sensor.

Several recent datasets with clearly visible LEE backgrounds are shown in **Figure 2***a*, from the BULLKID, CRESST, NUCLEUS, TESSERACT, and SuperCDMS-CPD experiments. We detail the measurements and experiments below.

**3.1.1. CRESST.** The CRESST-III experiment searches for nuclear recoils induced by low-mass DM particles in absorber crystals operated at millikelvin-scale temperatures in a low-background setup located deep underground at the LNGS facilities in Italy. Particle interactions in the crystal generate phonons, which are measured by W-TESs with aluminum phonon collectors, both evaporated directly on the crystals' surface with a SiO$_2$ layer in between. In its first dedicated

low-threshold data-taking campaign (3), the CRESST-III experiment operated $CaWO_4$ absorber crystals with individual masses of 24 g. The best-performing detector achieved a nuclear recoil threshold of 30 eV. An LEE was clearly visible in this detector, starting at $\lesssim 200$ eV and rising toward the threshold. This observation was confirmed by four other detectors in the same run with thresholds also below 100 eV. Despite the presence of this LEE, leading limits were set for DM masses <1 GeV. For a detector of the same performance, but without an LEE, these limits would be up to two orders of magnitude stronger (70).

Consequently, studying this LEE was a top priority for a measurement campaign that ran from 2020 to 2024. Detectors with different target materials, including $Al_2O_3$, $LiAlO_2$, and Si, in addition to $CaWO_4$, were operated. Several modules had further modifications to their design, such as different holding structures and surrounding materials, to test their impact on the LEE (43). The CRESST-III energy spectra in **Figure 2a** show that the LEE was observed across different targets and cannot be attributed to an effect of a single material. It is observed in detectors with different geometries—wafer (20 mm × 20 mm × 0.4 mm) or bulky (20 mm × 20 mm × 10 mm)—and the count rate of the currently dominating LEE component does not seem to scale with the target mass. Moreover, $CaWO_4$ crystals of different origins were used with no significant difference in the LEE rate observed (43). In all detectors, the LEE rate decays with time since cooldown, with decay times of $\mathcal{O}(100)$ days (for details, see Section 4). Triggered by the observations from the EDELWEISS experiment (1), the CRESST Collaboration performed a series of warm-up tests to different temperatures (60 K, 600 mK, and 200 mK); results are shown in Section 4. The CRESST experiment found that warm-ups to temperatures of $\mathcal{O}(10)$ K or higher enhance the LEE rate, which then decays with a fast [$\mathcal{O}(10)$ days] component before the previously observed slow decay component of $\mathcal{O}(100)$ days resumes. The CRESST experiment currently operates detectors with two TESs on the target crystal (double-TES) to disentangle events originating from a single TES or its interface to the crystal from events in the bulk (63). Details and first prototype data are discussed in Section 4.1.2.

### 3.1.2. NUCLEUS.
The NUCLEUS experiment aims to measure CEvNS from reactor antineutrinos (71). It employs gram-scale $CaWO_4$ and $Al_2O_3$ cryogenic detectors, equipped with W-TES sensors to achieve low-energy thresholds. The LEE spectrum from a prototype measurement by a 0.5-g $Al_2O_3$ detector operated at the surface with a 20-eV threshold is shown in **Figure 2a**. The same $Al_2O_3$ target crystal was later operated held by two thin Si wafers, each equipped with its own TES (72). This instrumented inner-veto system acts as both a surface veto and an instrumented holder. Given the expected moderate phonon transmission across the mechanical contact between the target and the inner veto, events originating in the veto wafers or on the crystal–holder interfaces are expected to exhibit different energy sharing between the target and veto TESs compared to events originating within the crystal volume, such as particle recoils. The low-energy spectrum was efficiently cleaned up using this veto cut (72). More recently, the NUCLEUS experiment operated an $Al_2O_3$ target crystal directly instrumented with two TESs (64). Similar to observations in the CRESST experiment, two distinct populations of LEE events were identified: one exhibiting equal energy sharing between the two sensors, the other in anticoincidence between the sensors.

### 3.1.3. SuperCDMS-CPD.
The SuperCDMS-CPD experiment deployed a 10.6-g Si target (1 mm thick with a surface area of 45.6 cm²) equipped with a single channel of 1,031 QETs. The setup was shielded by 5 cm of copper in an aboveground laboratory. An energy resolution of 3.86 eV was reached, allowing for an analysis threshold of 16.2 eV (33). The recoil energy spectrum (**Figure 2a**) clearly shows a strong rise toward lower energies.

### 3.1.4. TESSERACT.

TESSERACT, also known as SPICE and HeRALD (73), is a multitarget light DM experiment using QETs attached to a crystal substrate, which form either DM detectors (e.g., $Al_2O_3$, Si) or readout for separate DM targets (e.g., He, GaAs). The collaboration has demonstrated phonon energy resolutions as low as 375 meV in its phonon detectors, which measure bursts using two-channel arrays of many QETs to suppress LEEs through multichannel coincidence (45). The TESSERACT experiment has shown that glued-down detectors host large LEE populations, whereas suspended detectors (e.g., from wire bonds—low-stress holding) exhibit a lower residual LEE background (53). The spectrum measured in the low-stress configuration is shown in **Figure 2a** and further discussed in Section 4.1.1. In separate studies, the TESSERACT Collaboration showed that this residual population was composed of two components: energy depositions in the absorber crystal ("shared" LEE) and energy depositions in the metal films from which the phonon sensors are constructed ("singles" LEE) (45). Finally, the TESSERACT experiment has observed signatures of LEE-related processes (phonon coupling, multichannel correlation, relaxation with time) in excess noise that limits the resolution of the phonon detectors, indicating that understanding and reducing LEE backgrounds may be key to improving low-temperature sensor performance for, e.g., astronomical applications and axion searches as well.

### 3.1.5. EDELWEISS.

The EDELWEISS experiment deployed a 33.4-g ultrapure Ge absorber with a diameter and height of 20 mm, sensed with a Ge-NTD thermistor measuring 2 mm × 2 mm × 0.5 mm, glued to the top surface of the absorber. Electrical contacts were made using Au wires bonded to the Ge-NTD on one side and to Au pads deposited on a Kapton tape glued to the copper housing of the detector on the other. The low-energy spectrum from this detector is shown in **Figure 2a**. By additionally reading out ionization signal, the EDELWEISS experiment demonstrated that a significant fraction of its background down to at least 15 $eV_{ee}$ comes from events that lack an ionization signal and consist of heat only (HO) (9). Furthermore, the EDELWEISS experiment was the first to observe a strong decrease in the respective excess rate after the beginning of a cooldown (see Section 4) before reaching a steady rate. The EDELWEISS Collaboration also ruled out the possibility that a single source could explain the observed HO event rate, partly due to the steady HO excess rate observed in all runs and the abrupt variations in the HO rate observed in only some of the runs (66). While not covered in detail here, the EDELWEISS experiment separately operated Ge-HV charge detectors with results (9) similar to those discussed in Section 3.2.

### 3.1.6. RICOCHET.

RICOCHET is a planned experiment to search for CEνNS interactions in Ge detectors operated near a nuclear reactor in France. In the CryoCube detector concept, phonons are read out with NTD sensors glued to the detector surface, while charge is separately read out using high-electron-mobility transistor (HEMT) amplifiers. A prototype measurement operated three 38-g Ge crystals (30 mm in diameter, 10 mm high) at 15 mK, achieving a 30-$eV_{ee}$ ionization energy resolution (68). Each crystal featured planar aluminum electrodes covering the top and bottom surfaces, with a $(2 \times 2)$ $mm^2$ NTD sensor centered on the top electrode. LEE events were observed up to keV energies, significantly higher than in other experiments, and dominated by HO events as in previous EDELWEISS measurements. Using dual phonon and charge readout, the RICOCHET Collaboration strongly constrained ionization associated with LEE events, an observation that is now believed to hold generally for phonon LEE backgrounds.

### 3.1.7. BULLKID.

The BULLKID experiment operates an array of 60 MKIDs attached to a joint 3-inch Si wafer of 5-mm thickness. The wafer has notches in the shape of a rectangular grid, such that each sensor is most sensitive in an individual die of 0.34 g. A low-energy background spectrum recorded in 39 h of surface data with an energy threshold of 160 ± 13 eV is

shown in **Figure 2a** (35). After data quality and coincidence cuts between dies, a flat background of $2.0 \pm 0.1$ (stat.) $\pm 0.2$ (syst.) $\times 10^6$ dru remains, with no observable rise toward lower energies. Further study will determine whether this is due to an intrinsic property of the BULLKID detector or MKIDs that makes them resilient against the sources of LEE backgrounds seen by other detectors described here, or whether such LEE backgrounds are simply subdominant to the large flat background rates in the BULLKID surface detector.

**3.1.8. Superconducting quantum devices.** QP populations exceeding the thermal state of the superconductor have also been found in superconducting quantum devices. QPs are created by energy depositions that exceed the binding energy of Cooper pairs—for instance, $2\Delta \sim 87$ GHz $\times \hbar \sim 0.36$ meV in aluminum films (74). The thermal production of QPs at typical operation temperatures of about 10–40 mK is strongly suppressed, such that one would expect to observe less than a single QP in an Earth-sized aluminum volume. However, typical QP densities observed experimentally in aluminum are on the order of 0.01–10 $\mu m^{-3}$, as calculated from typical tunneling rates in Josephson junctions of hertz-to-kilohertz scale. The tunneling rate depends approximately linearly on the QP density in the junction and on the properties of the junction itself, such as dimensions and purity (75). The presence of such excess QPs is evidence for athermal interactions. Reference 69 provides a detailed study of the QP density on a micrometer-scale aluminum island, connected through a tunnel junction to a copper ground plane. The QPs in this study were sensed through a capacitively coupled single-electron transistor. The measured QP density features a decaying time dependency since the cooldown of the setup, similar to the decaying LEE backgrounds measured in other low-threshold detectors. Potential origins and mitigation strategies for these excess QPs are discussed in Section 4.3.

## 3.2. Low-Energy Events in Charge Detectors

Colloquially, the measured single-electron rate in a charge-sensitive detector is often referred to as a dark rate. However, this rate inherently includes both the sum of the true dark rate and any LEE contributions. Many sources of single-electron events can come from imperfections in detector design and not from external energy deposition or internal energy release. Dark rate strictly refers to single $e$–$h$ pair production in the absence of a localized energy source. We define single-electron LEE rates as any additional sources of events on top of dark rate contributions. The progression of single-electron rates measured in various Si charge detectors over time is shown in **Figure 2b**.

In contrast to phonon LEEs, where a single effect might have dominated LEE observations, the low-threshold charge detector community has made considerable progress in mitigating single-electron rates by identifying the following distinct contributions:

- Infrared (IR) radiation, such as from warm components in the same volume as the detector (e.g., a room-temperature vacuum vessel), can generate single $e$–$h$ pairs and leak into detector housings otherwise thought to be light-tight.
- High-energy particles from cosmic rays or background radioactivity can, through various processes, create low-energy optical photon bursts (76).
- CCD readout can induce spurious charge events, which can largely be mitigated through detector design and operation.
- Charge can thermally ionize at the relatively high temperatures ($\sim$140 K) at which CCDs are operated; this component is negligible for cryogenic HV detectors.

**3.2.1. SuperCDMS-HVeV.** The SuperCDMS R&D HVeV detectors are sensitive to single $e$–$h$ pairs by exploiting NTL amplification (see Section 2.2). Made of high-purity Si crystals (10 mm $\times$ 10 mm $\times$ 4 mm, 0.93 g), one crystal face is patterned with QETs in two readout channels to

collect phonons, while the opposite face has an aluminum grid. The QETs are grounded, and the grid can be biased with high voltage (~100 V), creating a uniform electric field. The first HVeV detector achieved a threshold of ≤0.8 $e$–$h$ pairs in the Run 1 DM search (6) and was outperformed by the following HVeV generations. The second generation of HVeV detectors increased the QET coverage from 13% up to 50% using different QET configuration masks and omitted a 40-nm amorphous Si layer. Initially, it was believed that this layer would reduce the probability of charge leakage from the bias electrodes into the crystal. However, tests showed that leakage did not significantly increase when the QETs were printed directly onto the crystal surface, leading to the omission of the layer in later generations. Both Runs 1 and 2 were conducted on the surface, at different locations and with different shielding, with the crystal clamped between two printed circuit boards (PCBs) for electrical connections and heat sinking. The observed event rates were comparable in both runs (62).

The Run 2 detector was also used for a zero-volt (0VeV) run to probe nuclear recoils, instead of electronic interactions, down to ~10 eV (77). Additional analysis of the 0VeV data led to the understanding that a contribution to the LEE is consistent with luminescence events from the PCBs (see Section 5.1). In HVeV Run 3, four detectors were mounted in pairs on two copper holders, operated at the Northwestern Experimental Underground Site (NEXUS) with an over-burden of 255 mwe (48). Each detector was clamped between two PCBs facing the neighboring detectors. Most of the events observed in Run 3 were coincident in multiple detectors, suggesting that external sources are dominating over internal sources (such as mechanical stress) in this run. Data recently taken at NEXUS with a new detector housing without PCB confirm that this background from luminescence can be successfully mitigated, reducing the LEE at higher energies. However, these data also indicate that a sensitivity-limiting LEE is still present at the lowest energies of interest.

### 3.2.2. DAMIC at SNOLAB.

The progression of CCD experiments over the years has largely focused on the reduction of single-electron rates alongside improved shielding to reduce radio-genic backgrounds. This began with the Dark Matter in CCDs (DAMIC) experiment, which released its first results in 2011 (78). Following this result, the DAMIC Collaboration designed a larger, low-background detector named DAMIC at SNOLAB, which released its first results in 2016 (79). This experiment was then upgraded with lower-background materials and more CCDs (for a total Si mass of 42 g), which released results for 11 kg-days of exposure in 2020 (80). Among other observations, this dataset included the first observation of a spatially uniform bulk LEE above modeled backgrounds (81) at energies below 200 $eV_{ee}$. To further investigate this LEE, the DAMIC Collaboration (working with the SENSEI and DAMIC-M Collaborations) upgraded DAMIC at SNOLAB with skipper CCDs to push to lower thresholds to probe this LEE signal. In 2023, the DAMIC Collaboration confirmed the presence of the bulk LEE in a different set of CCDs with a 23-$eV_{ee}$ threshold in 3.25 kg-days at >3$\sigma$ significance (55). This LEE seems sys-tematically different from the other LEE backgrounds in charge detectors, and a DM-type origin cannot be excluded from its own properties.

### 3.2.3. SENSEI.

The Sub-Electron Noise Skipper-CCD Experimental Instrument (SENSEI) Collaboration built on the success of the DAMIC experiment by pioneering the skipper CCD technology, with which the charge of each pixel can be measured to subelectron precision (82). Over several years, the SENSEI experiment has reduced the single-electron background rate from 1.14 $e^-$ per pixel per day in 2018 (56) to $1.39 \times 10^{-5}$ $e^-$ per pixel per day in 2024 (59). This reduction, and the corresponding reduction of two-electron backgrounds, is shown in **Figure 2b** and converted into mass-dependent rates to remove the effects of differing CCD thicknesses over the years. Gradual improvement was achieved through better shielding and reduction of light leaks

in the CCD housings. The improved shielding reduced the environmental radiation, which was shown to produce low-energy photons from Cherenkov radiation that can create single-electron events (76). The most recent measurements (59) suggest that there is only a mild excess of single-electron events over thermal excitation backgrounds remaining at SENSEI, which is expected to be reduced further in future measurements.

In Reference 58, the SENSEI Collaboration observed four three-electron events, while the expectation from the pileup of single-electron events was zero. Two of the three-electron events appeared in pixels that were likely affected by detector defects, but the origin of the other two is unknown. More data are needed to determine their origin.

**3.2.4. DAMIC-M.** The DAMIC at Modane (DAMIC-M) project represents the next stage in the CCD DM experiment progression, with plans to scale up to 1 kg of skipper CCD mass in a 0.1-dru low-background environment. Meanwhile, the DAMIC-M prototype low-background chamber (DAMIC-M LBC) (83) has already begun producing results (60). Soon, the DAMIC-M LBC will accumulate sufficient exposure to test the bulk LEE observed at DAMIC at SNOLAB in a different environment, but with similar CCDs, providing a strong test of possible radiogenic origins, such as neutrons. Meanwhile, the LBC has achieved initial single-electron rates of $4.5 \times 10^{-3}$ $e^-$ per pixel per day (84) with improvements expected in the next year.

**3.2.5. CONNIE.** The Coherent Neutrino-Nucleus Interaction Experiment (CONNIE) uses skipper CCDs for reactor CEνNS detection and has recently characterized a background (reactor-off) single-electron rate of $4.5 \times 10^{-2}$ $e^-$ per pixel per day (61). While slightly higher than the single-electron rates measured by the CCD DM experiments, this rate is notable due to the higher-radiation environment present in a reactor and provides valuable input on the radiation-induced component of single-electron LEEs.

## 4. ORIGINS OF PHONON EVENTS

Early work by the EDELWEISS Collaboration (66) and more recent studies by the CRESST Collaboration (43) have demonstrated that the rate of LEE backgrounds in a given energy bin decreases over time. Subsequently, further observations of decaying LEE rates have been reported at various detectors (53, 63, 65). This effect is illustrated in **Figure 3a**, where the LEE rates in several experiments are shown against time since cooldown. In the CRESST experiment, measurements were performed using different absorber materials, while for the TESSERACT experiment, the data shown in **Figure 3a** are split into two energy ranges. In addition to these TES-based phonon detectors, **Figure 3a** includes data on the rate of Cooper pair-breaking events in a mesoscopic superconductor device (69). The data from the TES-based detectors are well-described by exponentially decaying functions, as shown in the original studies (43, 53). However, the resulting decay times vary significantly, ranging from several days for data taken immediately after the cooldown to hundreds of days for those taken several months later. To account for this variability, we fit all experimental data with a power-law function, $\propto t^p$. For the phonon detector data, both functions fit equally well, possibly due to the large spread of the data points. The data from quasiparticle tunneling can only be described well with a power-law model. Overall, the power-law function provides a consistent description across all considered experiments. The resulting power-law exponent, $p$ (see labels in **Figure 3a**), ranges from $-0.43$ to $-0.96$ with a weighted mean of $-0.9 \pm 0.1$. Whether time is defined from the start of the cooldown or from reaching the base operating temperature substantially influences these fit results. Within the same cooldown, variations are observed in LEE rates across different energy ranges (e.g., a faster decrease at lower energies in the TESSERACT detector) and in different absorber materials (e.g., a slower decrease in CRESST $Al_2O_3$ versus $CaWO_4$ and Si).
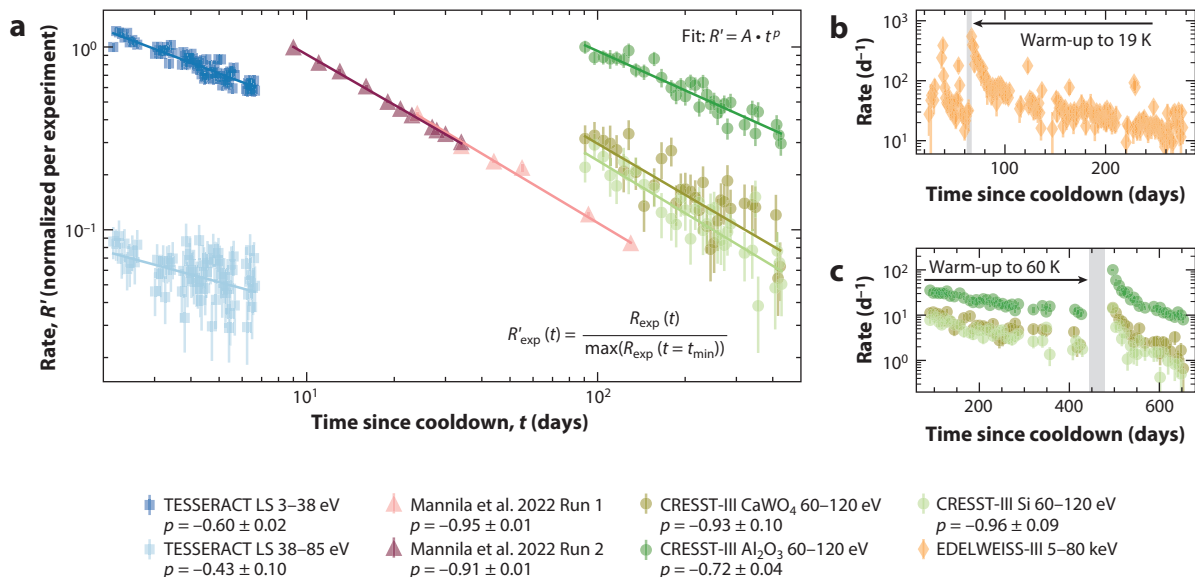
**Figure 3**

LEE rate evolution with time. Low-energy excess rates ($R'$) as a function of time since cooldown ($t$) for various experiments: TESSERACT LS configuration (Si, W-TES, surface) (53), Mannila et al. (Al, quasiparticles, surface) (69), CRESST-III (CaWO$_4$/Al$_2$O$_3$/Si, W-TES, LNGS) (43), and EDELWEISS-III (Ge, NTD, LSM) (66). (*a*) LEE rates in experiments with sufficient exposure decrease over time. The measured rates are analyzed for each dataset separately and fitted to a power law (*solid lines*). The normalization is floated such that the rate at the earliest time point in the dataset with the highest rate for the corresponding experiment is set to $R' = 1$. (*b*) Increase in the rate of heat-only events with energy ranging from 5 to 80 keV, observed in an EDELWEISS-III detector following a warm-up to ~19 K. (*c*) Segment of a dedicated temperature study by the CRESST Collaboration, showing an enhancement in the LEE rate after a controlled warm-up to 60 K. Abbreviations: LEE, low-energy excess; LNGS, Laboratori Nazionali del Gran Sasso; LS, low stress; LSM, Laboratoire Souterrain de Modane; NTD, neutron transmutation doped; W-TES, tungsten transition edge sensor.

The EDELWEISS Collaboration observed an increase in HO events after a warm-up of the cryostat to ~19 K (66) (**Figure 3***b*). A series of warm-up tests (partially shown in **Figure 3***c*) were later performed by the CRESST Collaboration. Despite strongly varying energy ranges (>5 keV for EDELWEISS and 60–120 eV in CRESST), both collaborations observed that warm-ups to tens of kelvins reenhance the LEE rate, which begins to decrease again with time once detectors return to their operational temperatures. The rate decay following such warm-ups appears to be faster than the initial decay with time since cooldown.

This behavior can be interpreted in different ways. One possibility is that warm-up procedures introduce transient effects that dissipate over shorter timescales. Alternatively, a faster decrease shortly after a detector reaches its operating temperature is expected naturally if the LEE rate follows a power-law decay over time, as discussed above.

The observations of the time decay of these phonon low-energy backgrounds are intrinsically incompatible with all hypotheses of common particle interactions due to their decay with time since the cooldown of the setup, leaving as possible origins solid-state physics effects that previously have been unaccounted for. Such effects could include the spontaneous or stimulated rearrangement of nonequilibrium atomic or electronic configuration within the detector or surrounding materials to a lower-energy state and subsequent transfer of energy to the detector phonon system. We elaborate on such ideas below, including stress, defect states, and excess QP population.
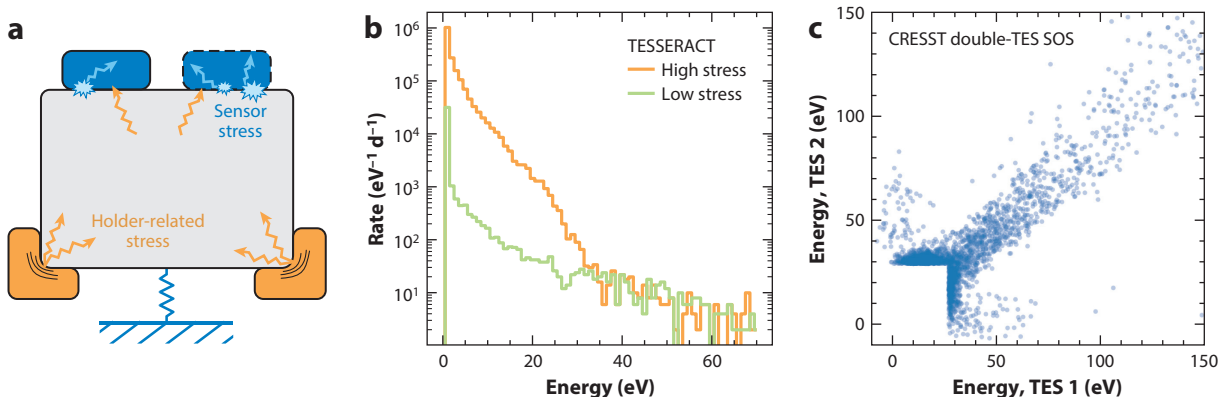
**Figure 4**

Stress-related LEE origins. (*a*) Schematic illustration of stress-related LEE origins, highlighting contributions from detector holders (*orange*) and phonon sensors (*blue*). (*b*) Energy spectra measured with a Si TESSERACT detector, showing a higher LEE rate in the high-stress configuration compared to the low-stress configuration. Panel adapted from Reference 53 (CC BY 4.0). (*c*) Scatter plot of energies measured by two TESs in an SOS double-TES CRESST detector operated at the surface (63), demonstrating the multicomponent nature of the LEE: events detected by both sensors (shared) and events with energy deposition in only one sensor (singles). Abbreviations: LEE, low-energy excess; SOS, Si on Sapphire; TES, transition edge sensor.

## 4.1. Stress

The cooldown of a cryogenic detector from room temperature to millikelvin-scale temperature induces thermal contractions in all materials and possibly shear stress on interfaces of components that contract differently. Since not all shear stress will immediately result in fractures or lattice reconfigurations, the remaining stress is a form of stored energy that can be released gradually over longer timescales, possibly inducing observable LEE events. Explaining discrete energy depositions of up to hundreds of eV via relaxation of shear stress through lattice reconfigurations requires the simultaneous rearrangement of many atoms, as a single-atom rearrangement is typically associated with smaller energy scales (e.g., ∼10-eV Frenkel defects in crystals). However, a comprehensive understanding and detailed description of this energy deposition mechanism remain to be developed. Systems with different material interfaces commonly found in phonon detectors (such as the crystal–holder or crystal–sensor film interfaces) are schematically illustrated in **Figure 4a** and discussed below.

**4.1.1. Detector-holding stress.** Early work by the CRESST Collaboration demonstrated that crystal fractures caused by very tight clamping can spontaneously release energies ranging from a few keV to several hundred keV (85). More recently, the TESSERACT experiment showed that certain detector-holding configurations are strongly correlated with LEE-type backgrounds (53). Specifically, the LEE rate was observed to be up to two orders of magnitude higher in a crystal operated under high stress (introduced by gluing it to a surface) compared to a crystal freely suspended on bond wires (see **Figure 4b**). However, more recent work by the CRESST Collaboration, in which a variety of sensor-holding schemes were investigated, showed that the observed low-energy background was insensitive to the exact holding method used (43). These results suggest that stress caused by the mounting scheme may not be the dominant mechanism behind the low-energy background in CRESST detectors. However, the detector-mounting process often lacks precise control over the level of induced stress. Experimental architectures with active holding, such as the i-sticks (86) previously used in the CRESST experiment, the instrumented Si inner veto developed by the NUCLEUS Collaboration (72), and the segmented BULLKID

monolithic detector array (52), are particularly well-suited for identifying holder-related stress events. Achieving sufficiently low thresholds in all subsystems in such designs could provide more insight into the role of holding-induced stress in LEE formation.

**4.1.2. Sensor stress.**  References 53 and 87 suggested that stress caused by differential thermal contraction of crystals and sensor metal films can be responsible for a part of the low-energy phonon background. Subsequent work by the TESSERACT (45), CRESST (63), and NUCLEUS (64) Collaborations focused on splitting the phonon readout into two channels by attaching a second phonon sensor to the same crystal. These studies identified events depositing equal energy in both sensors (shared events) and those detected almost exclusively in one channel (singles). This distinction allows singles to be excluded from the final energy spectrum. Data from one such measurement with a CRESST detector (63) are presented in **Figure 4c**. These singles can be interpreted as events occurring in the metal films themselves (45), potentially stress-induced or caused by other mechanisms, such as bursts of microwave photons entering the sensor via the bias lines (88). In contrast, shared events are less likely to result from relaxation in the metal films, as such relaxation is expected to deposit at least some energy locally (89). Instead, shared events are likely influenced by holder-related or intrinsic stress in the crystal as well as by stress at interfaces between the crystal and other instrumentation (e.g., bond pads, thermal links, electrodes).

If stress relaxation in sensor components contributes to the observed LEEs, the specific materials responsible have yet to be identified. Aluminum, widely used in phonon detectors, is a strong candidate (89), but other common materials (e.g., W, $SiO_2$, Au, Nb) may also play significant roles. However, comparing results across experiments remains challenging due to the need to isolate the sensor-related LEE component, compounded by variations in production methods, material sources, and the poor reproducibility that is often observed in thin-film fabrication.

## 4.2. Defect States

The lowest-energy state of a crystal lattice, the state of perfect symmetry, is never reached in a realistic crystal. Throughout the growth process, but also in any interaction of the lattice with its environment, lattice defects may accumulate. The relaxation of energy trapped in the crystal lattice in the form of defects has been hypothesized as a potential source of eV-scale energy depositions as phonon bursts (90). Defects that were created through interface stress, as discussed in Section 4.1, could act as such sites of stored energy. The impact of high-energy particles also can create defects that create ∼eV-scale energy depositions in their relaxation, as studied in Reference 91. As with stress-relaxation-induced backgrounds, also here an avalanche-like relaxation of many defects at once is required to explain the observed energies up to ∼100 eV. However, several questions remain unclear about this hypothesis, such as the long-term dynamics after the experiment's cooldown and the initial trigger for such an avalanche.

Crystals also are known to have defects (interpreted as trapped charges) in their structures whose configuration can resonate with microwave photons captured in quantum electronics and interact with electric fields and applied stress (92, 93). Interestingly, their configuration is observed to drift over time and reset after thermal cycling (94, 95). Devices sensitive to macroscopic energy scales observe these defects as a bath and noise with a $1/f$ frequency characteristic. The lifetimes of spin defects at low temperatures were observed to extend to months in $CaWO_4$ (96) and to hours in diamond (97). In addition, the surfaces of many crystals are known to undergo chemical reactions over time, such as oxidation or the adsorption of hydrogen at low temperatures. These processes could potentially release energy themselves—as is known, for instance, from the adsorption of $^4$He atoms on Si (73)—or change the likelihood of other reactions that deposit energy. We are

not aware of any studies regarding the evolution of surfaces of crystals on timescales of weeks in cryogenic low-pressure environments. A detailed study of the possible impact of all types of crystal defects on low-energy backgrounds is beyond the scope of this review.

## 4.3. Excess Quasiparticle Population

Many sources of athermal QPs have been studied in recent literature, such as vibrations (98), environmental radioactivity (99), and IR radiation (100). These studies mostly focus on the impact that QPs have on superconducting qubits, where they cause errors in quantum computations. While any interaction energy that exceeds the superconducting gap can create QPs, some origins are more critical than others due to high interaction rates or the creation of very high QP densities. The interaction of cosmic rays in the chip substrate (101, 102) is of special interest as such backgrounds are difficult to shield and deposit enough energy to cause very high QP densities across the whole chip and, therefore, correlated errors in multiple qubits that defeat error-correction algorithms. The absorption of IR photons through antenna modes of the circuit (103) and QPs from stress in the substrate from the sample packaging (53) have also been studied. IR photons are especially critical due to their high interaction rates. The dynamics of the QPs (once created) and their interaction with the qubit state were described in Reference 104. Mitigation strategies for excess QPs have been studied, including normal-metal traps for athermal phonons (105) and QPs (106), gap engineering of a potential barrier at the Josephson junction (107), and shielding from cosmic rays through operation in underground laboratories (108).

It is expected that the origins of the LEEs observed in phonon detectors also create QPs in quantum devices. The similar time dependence of QP tunneling and data taken with TES (see **Figure 3**) points in this direction and is discussed further in Section 6.

## 5. ORIGINS OF CHARGE EVENTS

Excess charge events can originate from primary or secondary radiation (**Figure 5**). This can include Cherenkov radiation, luminescence, blackbody radiation, Compton scattering, transition radiation, thermal dark rates, and spurious charge.
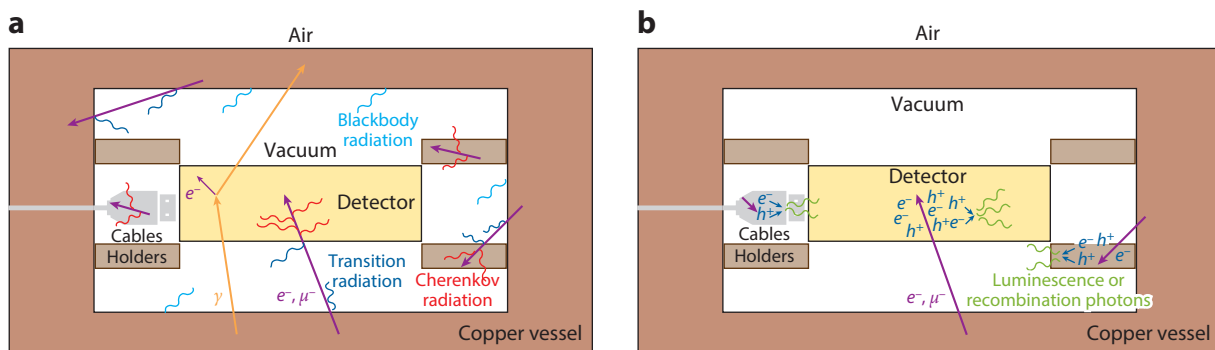


**Figure 5**

Charge backgrounds. Production of charge backgrounds in detectors through (*a*) primary radiation and (*b*) secondary radiation. High-energy charged particles (cosmic-ray muons or electrons) can either (*i*) pass through dielectric materials, such as the detector, the detector holders, or the cables, to produce Cherenkov radiation (*red*), (*ii*) cross surfaces to produce transition radiation (*dark blue*), or (*iii*) deposit energy in dielectric materials to create luminescence through, for instance, the recombination of electron–hole pairs (*green*). In addition, "warm" surfaces can produce blackbody radiation (*cyan*). In all cases the resulting radiation can be absorbed in the detector to produce a low-energy signal. Compton scattering of high-energy photons (*orange arrows*) can also produce low-energy electron recoils (*purple arrows*). Figure adapted from Reference 76 (CC BY 4.0).
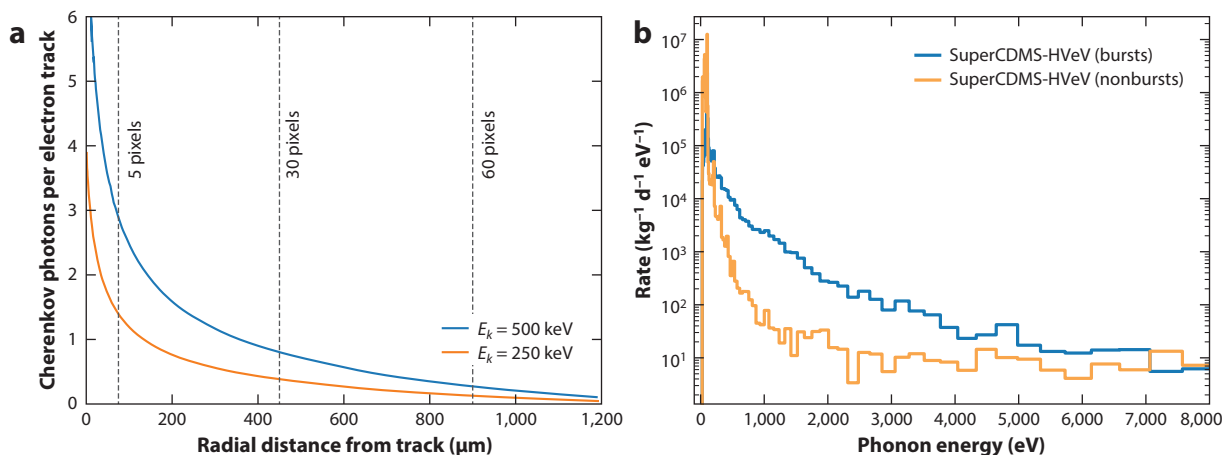
**Figure 6**

Charge-event background sources. (*a*) Number of Cherenkov photons emitted by one electron track passing through Si with energies of 500 keV (*blue*) and 250 keV (*orange*) versus the radial distance from the track. Vertical lines show the distance in pixels for skipper charge-coupled devices. Panel adapted from Reference 76 (CC BY 4.0). (*b*) Total phonon energy spectrum of burst events (*blue*) and nonburst events (*orange*) observed with a SuperCDMS-HVeV detector operated at 100 V. The reconstructed energy of the burst events is close to the energy of the primary pulse. Panel adapted with permission from Reference 110, with data from Reference 77.

## 5.1. Radiation-Induced Backgrounds

Here, we address sources of backgrounds in charge detectors that directly correlate with the rate of primary or secondary radiation incident on the detector.

**5.1.1. Cherenkov radiation.** Charged particles (from cosmic rays or radioactive contaminants) passing through dielectric materials can emit low-energy Cherenkov radiation that is absorbed by the detector and can mimic a DM event. In skipper CCD detectors, charged-particle tracks can be masked, but Cherenkov photons can travel and be absorbed far from the tracks to produce a single-electron event (76) (see **Figure 6a**). Two or more photons coincident in the same or neighboring pixels can mimic multielectron events. Cherenkov radiation also explains the spatial correlation between charged tracks and single-electron events observed in the SENSEI experiment (57, 109). Cherenkov photons can also be produced in dielectric materials near the sensor and be absorbed by it. This is a potential origin (76) of the two- to six-electron events observed in SuperCDMS-HVeV data (6). Cherenkov radiation backgrounds can be suppressed by improving the shielding and reducing radioactive contaminants.

**5.1.2. Luminescence.** Particles that traverse materials deposit energy in them, which may excite *e–h* pairs that create photons after recombination, a process commonly termed luminescence. This process can be prompt or delayed. As an example of delayed luminescence, $SiO_2$, the primary component of PCB as used in the original SuperCDMS-HVeV design (see Section 3.2.1), can emit luminescence photons of 4.4, 1.9, and 2.7 eV with decay times of 1.5 μs, 20 μs, and 7 ms, respectively (77). These energies and timescales can account for the excess of SuperCDMS-HVeV events featuring closely packed pulses in time, referred to as bursts (see **Figure 6b**). A burst consists of a distribution of primary events forming a single high-energy primary pulse and of secondary events quantized in one to three *e–h* pairs adding to the LEE.

**5.1.3. Infrared/blackbody radiation.** The energy thresholds of phonon and charge detectors are often well within the regime of sensitivity to single optical photons and below, such that

thermal radiation and other sources of IR photons can become sources of low-energy backgrounds. For detectors with higher thresholds, radiation of sub-eV photons is not resolvable on an event-by-event basis but can still be visible as shot noise and deteriorate the energy resolution given a sufficient power flux. Blackbody radiation has recently been identified by the SENSEI Collaboration as an important contributor to the single-electron event rate in data taken at SNOLAB and MINOS (59). Using a new design for the trays that hold the skipper CCD sensors with fewer light leaks, a reduced single-electron event rate was found. The hypothesis is that the warm surfaces inside the vessel that houses the trays emit blackbody radiation that can enter via light leaks and be recorded as a single-electron event. Additionally, the CCD amplifier can emit IR light during readout, which can be absorbed elsewhere in the CCD (7). Amplifier glow can be mitigated by optimizing the readout voltages and the amplifier design and turning off the amplifier voltages during exposure. Backgrounds compatible with room-temperature photons were furthermore observed with an optical TES in a subkelvin cryogenic setup in Reference 111. Thermal IR radiation is also among the sources of high excess QP rates observed in superconducting qubits (see Section 4.3).

### 5.1.4. Compton scattering.
Photons that undergo Compton scattering off electrons will produce electron recoils over a broad range in energies, including at the energies relevant for DM interactions (112–114). Careful control over radioactive contaminants and other environmental radiation is crucial for reducing this background to negligible rates. We note that Compton scattering does not explain the LEE, as its shape is different, but it can produce low-energy events.

### 5.1.5. Transition radiation.
Charged particles that traverse an interface that separates two different materials can produce transition radiation. This can occur when traversing two dielectric media or even a copper–vacuum interface. The number of photons emitted by a transition is far smaller than the number of Cherenkov photons produced by a charged particle traversing a dielectric material, but (unlike for Cherenkov radiation) there is no energy threshold for the charged particle. This radiation can be absorbed by a DM sensor and mimic a DM event (76, 115).

## 5.2. Fundamental Backgrounds

Additionally, charge detectors are expected to have fundamental background rates as determined by thermal excitations and readout electronics.

### 5.2.1. Dark rates (thermal).
True dark rates are generated from thermal fluctuations even if the detector is in complete darkness and perfectly isolated from its environment. In a CCD, there are various possible sources, including surface dark current, depletion dark current, bulk dark current, and diffusion dark current (49). High-quality Si can reduce the bulk dark current dramatically, while surface dark current can be reduced through the careful choice of CCD operational parameters. Nevertheless, some dark current will remain at finite temperatures and is exponentially suppressed for lower temperatures. The general dark current formula for a Si CCD with pixel area $A$, dark current figure of merit $D_{\mathrm{FM}}$, and band gap $E_{\mathrm{gap}}$, operating at a temperature $T$ (in kelvins), is given by (49)

$$D_R \simeq 5 \times 10^{13} \, \frac{e^-}{\text{pixel day}} \, \frac{A}{(15 \ \mu\text{m})^2} \, \frac{D_{\mathrm{FM}}}{0.1 \ \text{nA}} \, T^{3/2} \, e^{-\frac{E_{\mathrm{gap}}}{2 k_B T}}, \qquad 1.$$

where $k_B$ is the Boltzmann constant. For illustration purposes, we use $D_{\mathrm{FM}} = 1$ pA as this is roughly the value needed to match the upper limit set by the bulk dark rate in figure 10 of Reference 57, although it is most likely an overestimate of the true thermal dark rate (this is the dashed line shown in **Figure 2b**). In any case, we see that the dark current is very small for typical CCD operating temperatures. Thermal dark rate is negligible for a cryogenic detector operated below a few kelvins.

**5.2.2. Spurious charge.** Spurious charge in a CCD is generated when clocking the pixels, that is, when transferring charges between the pixels (49). It is spatially uniform and independent of the exposure, and the accumulated spurious charge depends on the number of times a pixel is clocked. Its average contribution can be subtracted from the exposure-dependent single-electron contribution (116), and it can be reduced by optimizing the clock voltages.

## 6. DISCUSSION AND OUTLOOK

Understanding and mitigating LEEs is an extremely important task for further sensitivity improvements in low-threshold DM and CEvNS experiments, as illustrated in **Figure 7** for the case of the DM nuclear recoil exclusion power. The main takeaways are as follows:

- The shape of the LEE matters. A steep LEE will be more similar to the spectrum of a light DM particle and thus have a higher impact at low DM masses, and vice versa (**Figure 7a,b**, top subpanels).
- The rate of the LEE is crucial. This is demonstrated in **Figure 7b** (bottom subpanel), which shows that an elevated LEE negatively affects the sensitivity over the whole DM mass range.
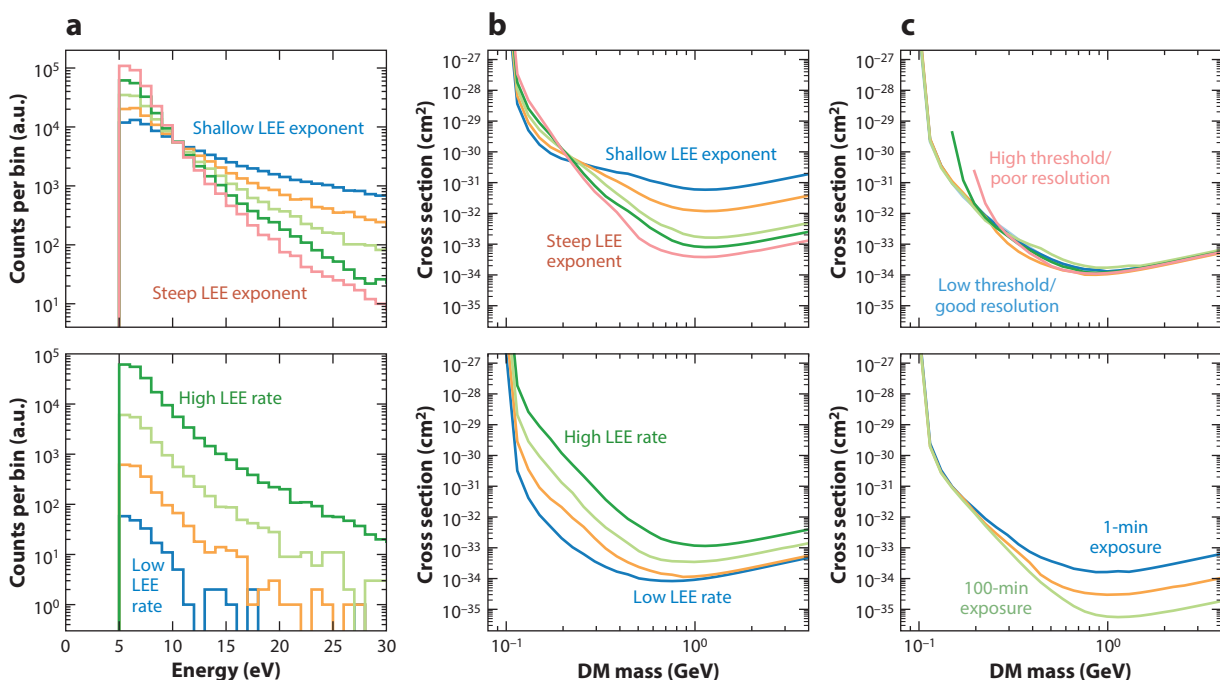


**Figure 7**

Simulations of the LEE's impact on DM limits. Spin-independent DM–nucleon projected limits for a 1-g Si detector, assuming a single power-law background $r_0\left(\frac{E}{1\,\mathrm{eV}}\right)^{-\kappa}$. Unless otherwise stated, projected limits are for a detector with a resolution $\sigma = 1$ eV, a threshold of 5 eV, and an exposure of 60 s. (*a*) Simulated event spectra, varying the power-law and rate terms together (*top*; $\kappa = [2, 3, 4, 5, 6]$, $r_0 = [10^2, 10^3, 10^4, 10^5, 10^6]$ Hz eV$^{-1}$ at 1 eV) and rate (*bottom*; $\kappa = 5$, $r_0 = [10^2, 10^3, 10^4, 10^5]$ Hz eV$^{-1}$ at 1 eV). (*b*) Simulated projected limits given the backgrounds in panel *a*, with a 60-s exposure of a 1-g Si detector. Color coding is consistent in panels *a* and *b*; for instance, in the top subpanels, the orange lines correspond to events where $\kappa = 3$ and $r_0 = 10^3$ Hz/eV. (*c, top*) Simulated projected limits in a detector with a varying resolution [$\sigma = 3$ eV (*pink*), 2 eV (*dark green*), 1 eV (*light green*), 0.5 eV (*orange*), 0.3 eV (*dark blue*), and 0.2 eV (*light blue*)], a threshold of $5\sigma$, and a background of $\kappa = 5$ and $r_0 = 10^4$ Hz/eV. (*c, bottom*) Simulated limits with exposures of 1 min (*blue*), 10 min (*orange*), and 100 min (*green*). Abbreviations: DM, dark matter; LEE, low-energy excess.

- For background-limited/LEE-dominated experiments, a lower threshold (**Figure 7c**, top subpanel) or higher exposure (**Figure 7c**, bottom subpanel) might not improve the sensitivity. As expected, a lower threshold extends the sensitivity to lower DM masses, but the improvements for higher masses are modest. Similarly, increasing the exposure will not help for low DM masses, at which the sensitivity is limited by the LEE.

Both spin-independent DM–nucleus scattering and CEνNS have cross sections that scale coherently, assuming an equal number of protons and neutrons in the target nuclei. Since the energy spectrum produced by CEνNS from reactor neutrinos closely resembles that expected from a DM particle with a mass of 2.7 GeV/$c^2$ (117), the neutrino flux corresponds to the equivalent DM interaction cross section, and the LEE's impact on CEνNS detectors' sensitivity can be inferred from **Figure 7**. Similar statements apply to sensitivities for DM–electron scattering. For example, 1-MeV DM particles produce only single-electron events (as the transferred energy is below the two-electron threshold), and since no experiment has yet succeeded in subtracting these backgrounds, DM limits scale linearly with reductions in single-electron rates. Even for DM heavier than a few MeV, the signal predominantly consists of only a few electrons, unlike DM–nucleus scattering. Reducing one- and few-electron backgrounds will directly enhance sensitivity to sub-GeV DM.

One of the key findings of the concerted effort to understand and characterize the LEE is that the dominant sources appear to differ between phonon- and charge-sensitive detectors. However, the nature of these underlying sources is not fully understood. For phonon-sensitive detectors, compelling similarities are observed across very different experiments, including the energy scales at which the excesses occur (with the notable exception of EDELWEISS), as well as the time dependence and reenhancement of LEE rates after warm-up. Detectors with double-TES readout, operated in the CRESST, NUCLEUS, and TESSERACT experiments, exhibit strikingly similar distributions of double- and single-TES events (45, 63, 64), albeit at different energy scales. These observations rule out a particle (signal and/or background) origin for the LEE.

Moving forward, the path toward DM and CEνNS science is best pursued through a program of diverse small-scale R&D, combining focused efforts to test individual LEE models with broader initiatives to explore LEE in new regimes or with new tools. A set of LEE models exists with fairly well-defined predictions. For example, in the radiation-induced crystal defect relaxation model (91), the rate of LEE in the energy range of interest should significantly increase after or while the detector is exposed to large amounts of defect-creating radiation. In the aluminum relaxation model (89), the LEE rate should be lower for detectors with less aluminum than for those with more. Certainly, the observed decrease in LEE rates over time at operating temperature is one of the best hints regarding the nature of the LEE. A detailed investigation of LEE rates across different timescales, along with further studies on temperature dependence and the impact of cooldown speed, may provide more insight into the underlying processes. From the currently available observations, a set of ideas focused on the relaxation of stress induced on the crystal or at its interfaces with other detector components has emerged.

To address the stress on the target crystal caused by holding structures, two main strategies are being employed. The first relies on instrumenting the holding structures and rejecting holder-related events through a dedicated veto cut. The NUCLEUS Collaboration is developing a Si-holding structure equipped with a TES (118). Similarly, the CRESST Collaboration has adopted an active holder approach by gluing the target crystal to another instrumented crystal in its mini-beaker module design (119). The second approach focuses on reducing external pressure on the target crystal, as implemented in the TESSERACT experiment with crystals supported solely by bond wires (53) and in the CRESST experiment using a gravity-assisted holding scheme (119).

Detectors with double-TES readout have revealed a fraction of low-energy background events localized in a single phonon sensor, which can be identified and removed from the final energy spectra (45, 63, 64). Combining instrumented holders with the double-readout approach, as planned in the NUCLEUS experiment, might enable the identification of both sensor-related and holder-related LEE events. Stress-related LEEs are also expected to be suppressed for super-fluid He targets read out by solid-state phonon-based microcalorimeter arrays, since the target He cannot experience any stress. LEE events originating from stress in the microcalorimeters will be reduced by exploiting the mostly different hit patterns between particle events and stress-induced events. This approach is being taken in the HeRALD (73) and DELight (120) experiments.

Two new NTD-based detector designs have evolved from the EDELWEISS experiment: CRYOSEL (used by the EDELWEISS Collaboration) (121) and CryoCube (used by the RICOCHET Collaboration) (68). The CRYOSEL-CRYO50 prototype is a Ge crystal equipped with two sensors, an NTD thermal phonon sensor and a NbSi film sensitive to athermal phonons. The latter is designed to measure charge through the detection of NTL phonons and, thus, enables the identification of bulk ionizing events and consequently the rejection of HO background events, which are a major component of the LEE in the EDELWEISS experiment (see Section 3.1.5). Initial tests with IR laser pulses on CRYO50 demonstrate the potential of this sensor technology to achieve the crucial single $e$–$h$ pair sensitivity (121).

Another promising approach to shed light on the origin of sources for the LEE is provided by pulse-shaped discrimination, as predicted, for example, by MAGNETO-DM (122). MAGNETO-DM uses a diamond target with a Au phonon absorber instrumented with a magnetic microcalorimeter (MMC) (123) to collect athermal phonons after an energy deposition. This technique exploits the fast response times achievable with MMCs to distinguish between energy depositions in the crystal, the Au phonon absorber, and the MMC sensor, in addition to discriminating between electronic and nuclear recoil events (122). This will enable a characterization of events contributing to the LEE (observed in recent MAGNETO-DM data) and is expected to provide new insights.

These and other upcoming measurements may yield new insights, particularly clarifying whether each LEE background is driven by a single mechanism or by a small set of related effects. However, the shared characteristics of the observed LEEs may well arise from a semiuniversal property of condensed matter systems at low temperatures, with variations specific to each experiment. The availability of accurate models of the low-energy backgrounds can enable new searches for New Physics, especially when observations can be compared across datasets from multiple detectors, as was shown, for instance, in Reference 124. In the event that these backgrounds are intrinsic to cryogenic solid-state systems, a path forward may rely on the development of low-threshold sensors with directional discrimination between isotropic LEE backgrounds and a DM or CEvNS signal (125).

Parallel observations in quantum circuits made of similar materials and operating in similar environments (see, e.g., References 39 and 69) have revealed excess event rates with similar characteristics. The bursts of excess QPs observed in an Al island on Si (69) resemble the phonon excess background seen with TES detectors with Al absorbers on Si (126). Both show similar time decay rates (**Figure 3**) for recoils above 60 eV. Extrapolating the TES observations to lower energies, using an energy spectrum $\propto$ (energy)$^{-2.2}$, yields hertz-scale recoil rates in the 100–1,000 × Al gap (~0.18 meV). Assuming an ~1% phonon-to-QP collection efficiency (in the range of efficiencies cited in References 31, 44, and 127), these rates align with QP bursts in the Al island. This suggests a possible shared origin, though alternative explanations and other contributions, such as from thermal IR photons, cannot be ruled out. The origins and mitigation of excess quasiparticles are the focus of ongoing research given their impact on superconducting quantum computers.

For charge-sensitive detectors, **Figure 2b** shows how the single-electron (and two-electron) background rates have steadily been reduced. This has been achieved through a combination of characterizing their origins, improving the operation of the detectors, and reducing the environmental backgrounds. Indeed, several origins of low-energy charge events have now been linked to (high-energy) environmental backgrounds, including Cherenkov radiation, luminescence, Compton scattering, and transition radiation, and can be reduced through careful detector shielding and radiological control. Blackbody radiation can be reduced by removing light leaks in the sensor housing to avoid light from warm surfaces reaching the sensor. Dark rates from thermal excitations can be reduced by cooling the detector, and the expectation is that these can be reduced to negligible levels even for the CCD detectors, which need to be operated above 100 K. IR light from the CCD amplifier can and must be controlled. Spurious charge generated during CCD readout produces an exposure-independent single-electron rate, which can be separated statistically from an exposure-dependent rate generated by DM; however, additional work is needed to reduce it further to maximize the detector's sensitivity to DM.

The SENSEI experiment's next steps include reducing the spurious charge and the blackbody radiation. For the latter, an updated light-tight design of the CCD copper trays will be employed. The SENSEI Collaboration's goal of accumulating an exposure of $\mathcal{O}(100)$ g years requires some control over radiogenic backgrounds, well within what has been demonstrated. The DAMIC-M Collaboration aims to obtain an exposure of 1 kg year, which requires tighter control over radiogenic backgrounds than in the SENSEI experiment to avoid LEE rates in the DM signal range. Both experiments will generate sufficient exposure to independently probe the origins of the DAMIC at SNOLAB excess rates, which appear distinct among LEEs discussed here. Moving forward, the OSCURA experiment (128) will merge the global CCD effort for an exposure of ~30 kg years, placing stringent requirements on avoiding radioactive contaminants and environmental exposure. As part of this effort, the CCDs will be immersed in liquid nitrogen, which will help reduce blackbody radiation.

The SuperCDMS Collaboration has recently operated multiple HVeV detectors at the CUTE underground facility at SNOLAB with a detector design and placement dedicated to the characterization of the LEE. Six HVeV detectors are stacked in a light-tight tower with four of them in the same optical cavity. Two detectors have a new design that includes ultrathin insulating $SiO_2$ layers to inhibit charges tunneling through the interfaces between deposited metals and Si to reduce the single $e$–$h$ pair rate. The aluminum coverage also varies between some of the detectors to probe the impact of this quantity on the LEE. The results will inform the next steps in the SuperCDMS-HVeV program.

Years after their first observation, LEEs continue to limit the scientific reach of experiments using low-threshold detectors. However, notable progress has been made in understanding them, alongside continued, albeit slowed, scientific advancements. Uncovering the origins of LEEs will likely require collaboration across the material science, solid-state physics, and quantum science communities, fostering an open-minded approach to low-energy phenomena. In our view, the LEE community should remain optimistic that backgrounds at low energies will eventually be understood and mitigated through ongoing projects, restoring sensitivity to interactions at the eV scale and beyond. Furthermore, a deeper understanding of our detectors and the fundamental processes involved—an inevitable outcome of these efforts—may inspire new technological advancements.

## DISCLOSURE STATEMENT

## ACKNOWLEDGMENTS

## LITERATURE CITED

1. Adari P, et al. *SciPost Phys. Proc.* 9:001 (2022)
2. Armengaud E, et al. *Phys. Rev. D* 99:082003 (2019)
3. Abdelhameed A, et al. *Phys. Rev. D* 100:102002 (2019)
4. Angloher G, et al. *Eur. Phys. J. C* 77:637 (2017)
5. Strauss R, et al. *Phys. Rev. D* 96:022009 (2017)
6. Agnese R, et al. *Phys. Rev. Lett.* 121:051301 (2018). Erratum. *Phys. Rev. Lett.* 122:069901 (2019)
7. Abramoff O, et al. *Phys. Rev. Lett.* 122:161801 (2019)
8. Aguilar-Arevalo A, et al. *Phys. Rev. Lett.* 123:181802 (2019)
9. Arnaud Q, et al. *Phys. Rev. Lett.* 125:141301 (2020)
10. Kurinsky N, Baxter D, Kahn Y, Krnjaic G. *Phys. Rev. D* 102:015017 (2020)
11. Harnik R, Plestid R, Pospelov M, Ramani H. *Phys. Rev. D* 103:075029 (2021)
12. Knapen S, Kozaczuk J, Lin T. *Phys. Rev. Lett.* 127:081805 (2021)
13. Heikinheimo M, et al. *Phys. Rev. D* 106:083009 (2022)
14. Abbamonte P, et al. *Phys. Rev. D* 105:123002 (2022)
15. Essig R, et al. *Phys. Rev. Lett.* 109:021301 (2012)
16. Agnes P, et al. *Phys. Rev. Lett.* 130:101002 (2023)
17. Li S, et al. *Phys. Rev. Lett.* 130:261001 (2023)
18. Aprile E, et al. arXiv:2411.15289 [hep-ex] (2024)
19. Amole C, et al. *Phys. Rev. D* 93:061101 (2016)
20. Freedman DZ. *Phys. Rev. D* 9:1389 (1974)
21. Essig R, Mardon J, Volansky T. *Phys. Rev. D* 85:076007 (2012)
22. Essig R, et al. *J. High Energy Phys.* 1605:46 (2016)
23. Derenzo S, et al. *Phys. Rev. D* 96:016026 (2017)
24. Ibe M, Nakano W, Shoji Y, Suzuki K. *J. High Energy Phys.* 1803:194 (2018)
25. Knapen S, Lin T, Pyle M, Zurek KM. *Phys. Lett. B* 785:386 (2018)

26. Kurinsky NA, Yu TC, Hochberg Y, Cabrera B. *Phys. Rev. D* 99:123005 (2019)
27. Griffin SM, et al. *Phys. Rev. D* 103:075002 (2021)
28. Kaznacheeva M, Schäffner K. *J. Adv. Instrum. Sci.* 2024:514 (2024)
29. Agnese R, et al. *Appl. Phys. Lett.* 103:164105 (2013)
30. Armengaud E, et al. *J. Instrum.* 12:P08010 (2017)
31. Pröbst F, et al. *J. Low Temp. Phys.* 100:69 (1995)
32. Angloher G, et al. *Phys. Rev. D* 110:083038 (2024)
33. Alkhatib I, et al. *Phys. Rev. Lett.* 127:061801 (2021)
34. Irwin KD, et al. *Rev. Sci. Instrum.* 66:5322 (1995)
35. Delicato D, et al. *Eur. Phys. J. C* 84:353 (2024)
36. Temples DJ, et al. *Phys. Rev. Appl.* 22:044045 (2024)
37. Catelani G, Schoelkopf RJ, Devoret MH, Glazman LI. *Phys. Rev. B* 84:064517 (2011)
38. Diamond S, et al. *PRX Quantum* 3:040304 (2022)
39. Yelton E, et al. *Phys. Rev. B* 110:024519 (2024)
40. Fink C, et al. *Phys. Rev. Appl.* 22:054009 (2024)
41. Linehan R, et al. arXiv:2404.04423 [physics.ins-det] (2024)
42. Ramanathan K, et al. arXiv:2405.17192 [physics.ins-det] (2024)
43. Angloher G, et al. *SciPost Phys. Proc.* 12:013 (2023)
44. Fink CW, et al. *Appl. Phys. Lett.* 118:022601 (2021)
45. Anthony-Petersen R, et al. *Appl. Phys. Lett.* 126:102601 (2025)
46. Albakry M, et al. *Phys. Rev. Lett.* 131:091801 (2023)
47. Kluck H, et al. *J. Low Temp. Phys.* 218:101 (2024)
48. Albakry MF, et al. arXiv:2407.08085 [hep-ex] (2024)
49. Janesick JR. *Scientific Charge-Coupled Devices*. SPIE Press (2001)
50. Neganov BS, Trofimov VN. *Otkryt. Izobret.* 146:215 (1985)
51. Luke PN. *J. Appl. Phys.* 64:6858 (1988)
52. Cruciani A, et al. *Appl. Phys. Lett.* 121:213504 (2022)
53. Anthony-Petersen R, et al. *Nat. Commun.* 15:6444 (2024)
54. Aguilar-Arevalo A, et al. *Phys. Rev. Lett.* 118:141803 (2017)
55. Aguilar-Arevalo A, et al. *Phys. Rev. D* 109:062007 (2024)
56. Crisler M, et al. *Phys. Rev. Lett.* 121:061803 (2018)
57. Barak L, et al. *Phys. Rev. Lett.* 125:171802 (2020)
58. Adari P, et al. *Phys. Rev. Lett.* 134:011804 (2025)
59. Bloch IM, et al. arXiv:2410.18716 [astro-ph.CO] (2024)
60. Arnquist I, et al. *Phys. Rev. Lett.* 130:171003 (2023)
61. Aguilar-Arevalo AA, et al. arXiv:2403.15976 [hep-ex] (2024)
62. Amaral D, et al. *Phys. Rev. D* 102:091101 (2020)
63. Angloher G, et al. arXiv:2404.02607 [physics.ins-det] (2024)
64. Kaznacheeva M. *Exploring the sub-keV energy region with the CRESST and NUCLEUS experiments*. PhD Thesis, Technische Universität München (2024)
65. Underwood R. *Dark matter searches with germanium and silicon detectors in SuperCDMS and CUTE*. PhD Thesis, Queen's University (2022)
66. Queguiner E. *Analysis of the data of the EDELWEISS-LT experiment searching for low-mass WIMP*. PhD Thesis, Université de Lyon (2018)
67. Augier C, et al. *Phys. Rev. D* 108:022006 (2023)
68. Augier C, et al. *Eur. Phys. J. C* 84:186 (2024)
69. Mannila ET, et al. *Nat. Phys.* 18:145 (2022)
70. Angloher G, et al. arXiv:2505.01183 [astro-ph.CO] (2025)
71. Strauss R, et al. *Eur. Phys. J. C* 77:506 (2017)
72. Rothe J, et al. *J. Low Temp. Phys.* 199:433 (2020)
73. Anthony-Petersen R, et al. *Phys. Rev. D* 110:072006 (2024)
74. Douglass DH, Meservey R. *Phys. Rev.* 135:A19 (1964)

75. Kurter C, et al. *NPJ Quantum Inf.* 8:31 (2022)

76. Du P, Egana-Ugrinovic D, Essig R, Sholapurkar M. *Phys. Rev. X* 12:011009 (2022)

77. Albakry M, et al. *Phys. Rev. D* 105:112006 (2022)

78. Barreto J, et al. *Phys. Lett. B* 711:264 (2012)

79. Aguilar-Arevalo A, et al. *Phys. Rev. D* 94:082006 (2016)

80. Aguilar-Arevalo A, et al. *Phys. Rev. Lett.* 125:241803 (2020)

81. Aguilar-Arevalo A, et al. *Phys. Rev. D* 105:062003 (2022)

82. Tiffenberg J, et al. *Phys. Rev. Lett.* 119:131802 (2017)

83. Arnquist I, et al. *J. Instrum.* 19:T11010 (2024)

84. Arnquist I, et al. *Phys. Rev. Lett.* 132:101006 (2024)

85. Åström J, et al. *Phys. Lett. A* 356:262 (2006)

86. Strauss R, et al. *Nucl. Instrum. Methods Phys.* 845:414 (2017)

87. Zema V, et al. The low energy excess in CRESST-III. Presentation at the EXCESS23@TAUP Workshop, Aug. 26 (2023)

88. Romani RK, et al. *Appl. Phys. Lett* 125:232601 (2024)

89. Romani RK. *J. Appl. Phys.* 136:124502 (2024)

90. Pereverzev S. *Phys. Rev. D* 105:063002 (2022)

91. Nordlund K, et al. arXiv:2408.07518 [cond-mat.mtrl-sci] (2024)

92. Lisenfeld J, et al. *Nat. Commun.* 6:6182 (2015)

93. Bilmes A, Volosheniuk S, Ustinov AV, Lisenfeld J. *NPJ Quantum Inf.* 8:24 (2022)

94. Zanuz DC, et al. arXiv:2407.18746 [quant-ph] (2024)

95. Reiss Y, Schechter M. arXiv:2410.19930 [cond-mat.dis-nn] (2024)

96. Wang Z, et al. arXiv:2408.12758 [quant-ph] (2024)

97. Astner T, et al. *Nat. Mater.* 17:313 (2018)

98. Kono S, et al. arXiv:2305.02591 [quant-ph] (2023)

99. Vepsäläinen AP, et al. *Nature* 584:551 (2020)

100. Barends R, et al. *Appl. Phys. Lett.* 99:113507 (2011)

101. McEwen M, et al. *Nat. Phys.* 18:107 (2022)

102. Harrington PM, et al. arXiv:2402.03208 [quant-ph] (2024)

103. Liu CH, et al. *Phys. Rev. Lett.* 132:017001 (2024)

104. Martinis JM. *NPJ Quantum Inf.* 7:90 (2021)

105. Iaia V, et al. *Nat. Commun.* 13:6425 (2022)

106. Riwar RP, et al. *Phys. Rev. B* 94:104516 (2016)

107. McEwen M, et al. arXiv:2402.15644 [quant-ph] (2024)

108. Cardani L, et al. *Nat. Commun.* 12:2733 (2021)

109. Du P, Egaña Ugrinovic D, Essig R, Sholapurkar M. *J. High Energy Phys.* 2401:164 (2024)

110. SuperCDMS Collaboration. SuperCDMS public documentation: HVeV-0VeV cross analysis. *SLAC National Accelerator Laboratory*. **https://www.slac.stanford.edu/exp/cdms/ScienceResults/PublicDocsAndPlots/0VeV/PubDoc.html** (2022)

111. Manenti L, et al. *Phys. Rev. Appl.* 22:024051 (2024)

112. Botti AM, et al. *Phys. Rev. D* 106:072005 (2022)

113. Norcini D, et al. *Phys. Rev. D* 106:092001 (2022)

114. Essig R, et al. *Phys. Rev. D* 109:116011 (2024)

115. Robinson AE. arXiv:2010.11043 [astro-ph.IM] (2020)

116. Barak L, et al. *Phys. Rev. Appl.* 17:014022 (2022)

117. Billard J. *Searching for dark matter and New Physics in the neutrino sector with cryogenic detectors.* Habilitation Thesis, Université Claude Bernard Lyon 1 (2021)

118. Goupy C, et al. *SciPost Phys. Proc.* 12:053 (2023)

119. Angloher G, et al. *J. Low Temp. Phys.* 216:393 (2024)

120. von Krosigk B, et al. *SciPost Phys. Proc.* 12:016 (2023)

121. Lattaud H, et al. *J. Low Temp. Phys.* 215:268 (2024)

122. Kim I, et al. arXiv:2409.19238 [physics.ins-det] (2024)

123. Enss C, et al. *J. Low Temp. Phys.* 121:137 (2000)
124. Wagner F. *Towards next-generation cryogenic dark matter searches with superconducting thermometers.* PhD Thesis, TU Wien/Österreichische Akademie der Wissenschaften (2023)
125. Blanco C, Kahn Y, Lillard B, McDermott SD. *Phys. Rev. D* 104:036011 (2021)
126. Angloher G, et al. *Phys. Rev. D* 107:122003 (2023)
127. Benevides R, et al. *Phys. Rev. Lett.* 133:060602 (2024)
128. Aguilar-Arevalo A, et al. arXiv:2202.10518 [astro-ph.IM] (2022)